Bulletin of the Seismological Society of America, Vol. 84, No. 3, pp. 768–779, June 1994

Continuous Measurements of Crustal Deformation for the 1992 Landers Earthquake Sequence

by Frank K. Wyatt, Duncan Carr Agnew, and Michael Gladwin

Abstract We describe, and attempt to interpret, continuous measurements of strains and tilts made at Piñon Flat Observatory (PFO) before, during, and after the Landers and Joshua Tree earthquake sequences. These data show substantial transient deformation following the Landers mainshock, with a total amplitude of several percent of the co-seismic deformation, and a decay time of at least several days. Comparing data from the many types of instruments at PFO allows us to infer possible sources for this deformation. The immediate postseismic transient was nearly the same size on three long-base strainmeters, suggesting either broadscale deformation or local motion near one part of the observatory. The latter can largely be ruled out by the similarity of many other measurements in the area covered by these strainmeters and the observations by others of significant postseismic displacements nearer the source. Possible mechanisms for broad-scale deformation include postseismic fault slip, time-dependent creep in near-surface rocks, and elastic or thermal responses to water-table changes. The first two agree best with the observations from PFO, but if postseismic fault slip is the source, it must have been distributed differently than the co-seismic slip, and may have included faults other than those that ruptured seismically. If one of the other mechanisms is the main source, the PFO data imply that the postseismic slip must have been very much smaller than the seismic slip, perhaps 2% or less. No significant preseismic deformation was observed, at a level of 2×10^{-3} of the co-seismic deformation, for the days to minutes before the earthquake.

Introduction

Radiated seismic waves have provided considerable detail on the nature of fault motion during an earthquake, but much less is known about fault motion too gradual to radiate significant energy. Such slower motions can only be detected from the quasi-static deformations which they cause; since these deformations decay with distance from the source as r^{-3} (as opposed to the r^{-2} of radiated waves), they require deformation-measuring instruments to be near an earthquake, which is rarely true. Slower deformations might be expected to occur, both before and after rupture, for certain classes of fault models (Lorenzetti and Tullis, 1989); observations of them (or of their absence) can bound possible instability models for the initiation of fault rupture. For previous California earthquakes, Johnston *et al.* (1987, 1990), and Agnew and Wyatt (1989) have found no detectable slow deformation in the days to minutes before a shock, though Gladwin *et al.* (1991) did identify a change in deformation rate about a year prior to the 1989 Loma Prieta earthquake. Gladwin *et al.* (1987), Agnew and Wyatt (1989), Wyatt (1988), and Gwyther *et al.* (1992) have reported observations of postseismic deformation; in some cases these show transient strains over the hours to days following the rupture, though in others (most notably for the Loma Prieta shock) no short-term transient was seen.

In this article we discuss data from Piñon Flat Observatory (PFO) that provide one of the best examples yet of postseismic motion. PFO is a geophysical observatory designed (in part) to study the measurement and interpretation of crustal deformation over all time scales. It includes a large variety of strain and tilt measuring instruments; Table 1 lists these, while Figure 1 shows their locations at the observatory. Since PFO began operating in 1971, the largest earthquake to happen nearby (or indeed within California) was the Landers shock of 28 June 1992. The occurrence of a large earthquake this close to a varied set of high-quality deformation sensors is, so far as we know, unique; for this reason we feel that it is important to present the observations, even though

Table 1
PFO—Measurements Used

Name	Description	Length (m)	Depth (m)	Sample Interval	Reference
		Deformation Measurements			
LSM*	Long-base laser strainmeter	732	0	1 and 300 sec	Wyatt *et al.* (1982)
BTSM	3-comp. borehole strainmeter	0.125	151	1080 sec	Gladwin (1984)
UCSD LFT	Long-base fluid tiltmeter	651/544†	0	300 sec	Agnew (1986)
LDGO LFT	Long-base fluid tiltmeter	535‡	0	300 sec	Bilham *et al.* (1979)
KUB	Askania borehole tiltmeter	1.5	100	300 sec	Agnew (1986)
BOA/BOB	JILA borehole tiltmeters	0.5	24/36	300 sec	Kohl and Levine (1993)
PIN1/2	GPS displacement (PGGA)	—	0	1 day	Bock and Shimada (1990)
ROCH	GPS displacement (relative)	14,300	0	1 day	Happer *et al.* (1991)
Two-Color	EDM network	−3500§	0	1 to 3 months	Langbein *et al.* (1987)
		Continuous Ground-Water Measurements			
CIA	Borehole, water at 34 m	135¶	196	300 sec	
CIB	Borehole, water at 29 m	149	210	300 sec	
CIC	Borehole, water at 14 m	79	140	300 sec	
UQA	Borehole, water at 28 m	131	173	300 sec	

*NS LSM at azimuth 0°(clockwise from N); EW LSM at azimuth 90°; NW–SE LSM at azimuth 135°.
†651-m system at azimuth 106.3° (labeled EW); 544-m system at azimuth 0.5° (labeled NS).
‡At azimuth 107.3° (labeled EW).
§Average line length.
¶Length is that of uncased wellbore; all surface casings extend into the water.

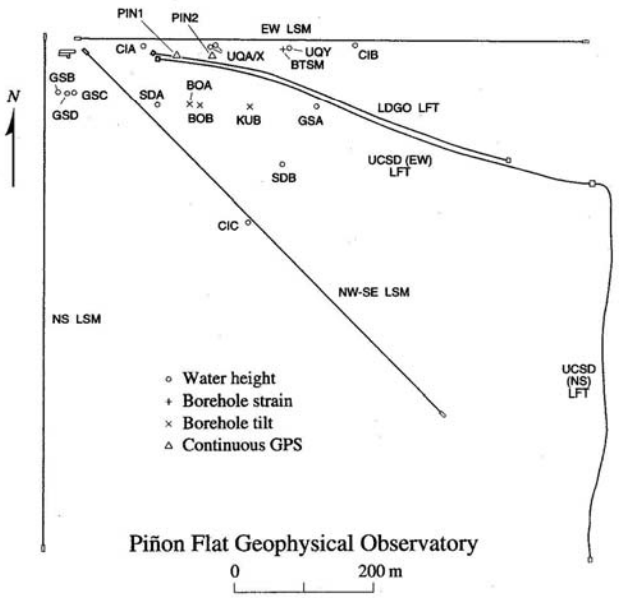

Figure 1. Site plan of PFO, showing the long-base and borehole instruments. Table 1 gives information on the various sensors.

they raise more questions than we currently have answers for.

Figure 2 shows the location of PFO relative to the Landers earthquake of 28 June 1992 (1992:180.499), and its rupture zones, both the mapped surface break and the aftershocks, the largest of which, the Big Bear earthquake (at 1992:180.630), is specially indicated. Figure 2 also shows the initial event of the complete sequence,

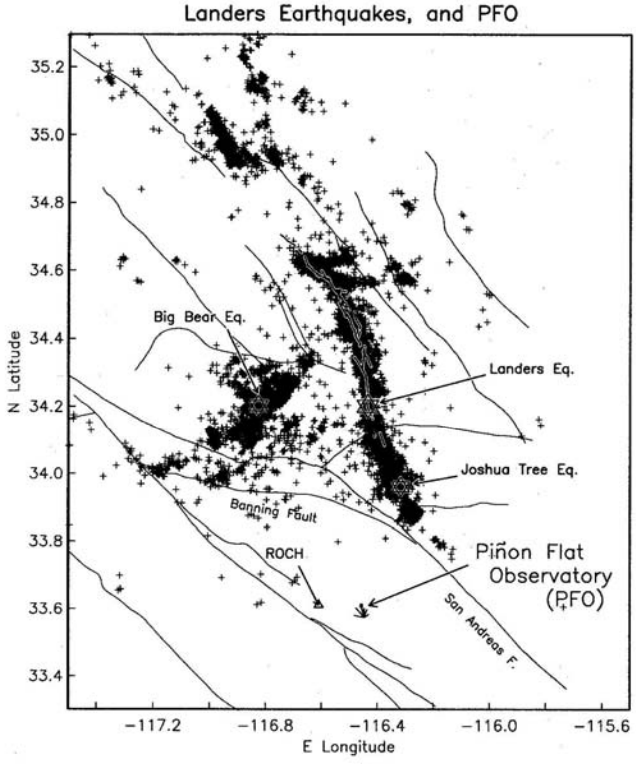

Figure 2. Map showing the location of Piñon Flat Observatory (PFO) relative to the Landers rupture. Earthquakes shown are for 1992, days 180 through 240, plus the Joshua Tree mainshock. The black-on-white line shows the surface break. ROCH is the location of a continuous GPS site (Fig. 11).

the Joshua Tree earthquake of 24 April (1992:114.201). PFO is within one fault length of the complete Landers rupture and only 43 km from the Joshua Tree earthquake.

Co-Seismic Deformations

For earlier earthquakes in southern California, far-field measurements of co-seismic strains and tilts have contributed significantly to moment estimates (e.g., Wyatt, 1988). However, for this earthquake sequence the displacement data nearer the rupture are so plentiful that they can determine the slip pattern and total moment much better (Hudnut *et al.*, 1994; Johnson *et al.*, 1994). It remains useful to examine the co-seismic data at greater distances to examine the validity of conventional elastic dislocation modeling; in seismological terms, given knowledge about the source, we can study the response of the earth to it.

The most reliable sources of co-seismic offset estimates at PFO have previously been the long-base strainmeters and tiltmeters. For the Landers earthquake this is only partly true. The UCSD long-fluid tiltmeters failed to track during the heaviest shaking, but the absolute tilt offset could be determined when they were reset a few hours later. The laser strainmeters suffered a brief loss of lock from a momentary power outage; in addition, the dynamic strains from the traveling waves were nearly 100 times their maximum design range. (Integration of the acceleration records from the TERRASCOPE system at PFO shows the peak horizontal velocity to have been about 0.5 m/sec; for a wave velocity of 5 km/sec this gives strains of 10^{-4}). Since the laser strainmeters are not absolute instruments, the co-seismic strains cannot be recovered from them. However, co-seismic strain estimates are available from two other sources: the borehole tensor strainmeter (BTSM) and a network of two-color EDM measurements made across Pinyon Flat under the direction of Dr. John Langbein of the U.S. Geological Survey. As part of regularly scheduled observations, this network was measured in May 1992; it was then remeasured in early July. Table 2 gives the co-seismic signals from the BTSM, the two-color EDM data, the UCSD long-base tiltmeters, and a deep borehole tiltmeter; also given are the computed deformations from the model of Hudnut *et al.* (1994).

Of the available estimates of co-seismic strains, we would normally regard the geodetic results from the two-color network to be the most reliable, and the data from the Pinyon network do show fair agreement with the model strains. Data from two other two-color EDM networks across the San Jacinto fault to the west of PFO (J. Langbein, personal comm.) match the model strains about as well as the Pinyon network does; it is notable that such agreement on and off the fault is not what would be expected if fault zones concentrate stress and strain.

The BTSM data and the two-color EDM data disagree with each other and with the model by about equal amounts; we note that some systematic error can be introduced into the BTSM values by inexact estimates of the effect of borehole coupling (Gladwin and Hart, 1985). The borehole coupling factors have been estimated using only the theoretical strain tides for PFO, and are thus almost certainly subject to systematic errors of 10 to 20%.

Table 2
Co-Seismic Deformations at PFO

Source	Type	Deformation			
Strains*		e_{11}	e_{22}	e_{12}	e_{NW-SE}
Two-color EDM, data†	Sum	−0.26 ± 0.19	0.92 ± 0.05	−0.69 ± 0.10	1.02 ± 0.14
Two-color EDM, model†,‡	Sum	−0.16	0.98	−0.43	0.84
Model‡	Landers	−0.15	1.02	−0.36	0.79
Model‡	Big Bear	0.024	0.034	−0.045	0.074
Model‡	Sum	−0.13	1.05	−0.40	0.86
BTSM	Landers	−0.23	1.05	−0.11	0.52
BTSM	Big Bear	0.012	0.062	−0.061	0.098
BTSM	Sum	−0.22	1.11	−0.17	0.62
Tilts§		Ω_1	Ω_2		
Model‡	Landers	0.381	−0.234		
Model‡	Big Bear	0.031	−0.001		
Model‡	Sum	0.412	−0.235		
LFT	Sum	0.332	−0.154		
KUB	Sum	0.185	−0.071		

*For all strain components, units are 10^{-6}, extension positive, and the 1-axis east, 2-axis north.

†Equivalent strain across network, computed from change of line lengths for both model and data.

‡From dislocation model of Hudnut *et al.* (1994), assuming a half-space response; except for the two-color network, evaluated at PFO (33.609° N, 116.455° W).

§For all tilt components, units are 10^{-6}; positive tilt for the direction given (footnote *) is that in which a plumb bob would move.

We note the good agreement between the BTSM and model results for the Big Bear shock; the BTSM data are one of the few constraints available on the static moment of this event. In a number of places we shall wish to compare the strains seen on the LSM's with the size of the co-seismic offset; admitting to some uncertainty, we have used for this the values calculated from the two-color EDM data.

Preseismic Signals

A number of frictional models of faulting predict that the final rupture should be preceded by a gradually accelerating slip. This has not been seen for any earthquake in California before the Landers event, and we did not see it for this earthquake either, even though there were clear foreshocks at the epicenter (Hauksson *et al.*, 1993). Figure 3 shows the last 300 sec before the Landers earthquake, including the initial *P* wave (which is off-scale on this plot). We show a bar to indicate 0.04% of the total co-seismic offset for the NW–SE strain; it is clear that this strainmeter limits any immediate preseismic slip to 2×10^{-4} of the co-seismic, an unprecedentedly small constraint. We also show the expected preseismic deformation for a fault-friction model (Lorenzetti and Tullis, 1989) with parameters set to give relatively small preseismic strains (less than 0.1%); the fact that we can rule this out indicates that any precursory deformation on the scale of the whole rupture must have been very small. Of course, this assumes that the whole of the final rupture was behaving uniformly. Abercrombie and Mori (1994) have reported that initiation of rupture began with a pair of subevents, magnitude 4.4 and 5.6; even for the larger of the two, we can set a limit of no better than 4% for the ratio of its precursory to seismic slip—generally too large to be useful in constraining models. Data over longer times (see below) show no precursory anomalies, except for a possible signal following the Joshua Tree shock.

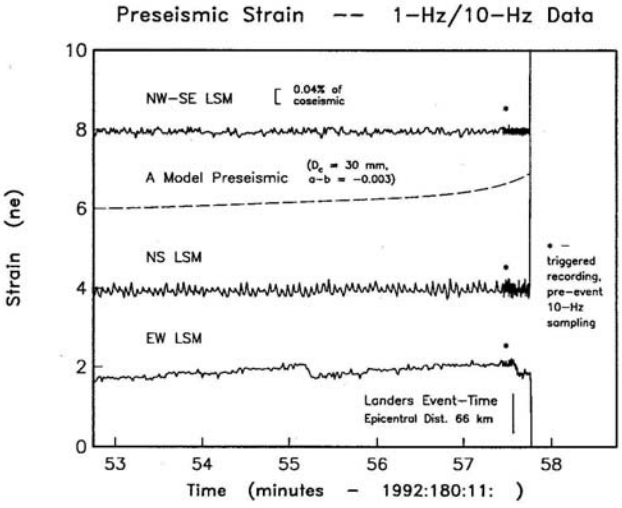

Figure 3. Records from the three laser strainmeters for the last 300 sec before the arrival of seismic energy from the Landers earthquake. The data are sampled once per second, except for the last 10 sec, which were recorded at 10 Hz and stored in a triggered pre-event memory. Microseisms are the source of the continuous fluctuations; the two rapid decreases in EW strain reflect mechanical stiction in its vacuum-pipe adjustment system. For comparison, the dashed line shows a representative model for preseismic strain release, though one that does not fit the data.

Postseismic Deformations

In the day following the Landers event, the telemetered records showed strain changes of unprecedented rapidity on all three laser strainmeters; the change in this day was about what is normally seen in a year. Some prompt data editing indicated that the rate of postseismic strain, while still rapid, was decreasing, reducing some concern in the community over a possible short-term hazard, but not interest in the nature and source of this signal. Earlier PFO data (Wyatt, 1988; Agnew and Wyatt, 1989) have often suggested rapid postearthquake strain, but never in such a large or long-lasting way. In this section we discuss the postseismic data, and in the next section the possible causes of these signals.

Figure 4 shows 60 hr of data on either side of the Landers earthquake for the three laser strainmeters (LSM's), with all co-seismic offsets set to zero. Here and in other figures we show data both with tides, for a sense of scale, and without, to expose the underlying behavior. It is evident that the strain rate, which before the Landers earthquake was very small, became very large right after it, with all three laser strainmeters showing a rapid extension that decreased with time, generally quite smoothly, though there appears to be a just-significant fluctuation, lasting a few hours, on all three instruments at about day 181.6.

Figure 5 shows the data from two of the BTSM sensors, with and without co-seismic offsets (including one from an aftershock at 181.65). While all three sensors of this instrument provided good values for the co-seismic strain, sensor number 2 is currently affected by spurious strain excursions, and we have therefore not presented it. We show data from the other two sensors; while each of these measures extension in one direction inside the borehole, it should be remembered that this does not simply correspond to a similar extension outside (Gladwin and Hart, 1985; Agnew, 1986). Even allowing for this, the data from these sensors is substantially different from what the LSM's imply: sensor number 1 shows a decaying strain contraction, opposite the sense of the LSM data, while sensor number 3 shows rapid strains between

the Landers and Big Bear events and little change in strain thereafter.

Once the radiated energy from the Landers earthquake arrived, measurements of the much smaller signals from quasi-static deformation became nearly impossible; the first meaningful measurements come about 30 min later. The first postseismic data are from the BTSM for strain, and from the borehole tiltmeters for tilt. The first laser-strain data come about 80 min after the Landers shock. These data provide bounds on the deformation for the 2.5-hr period just before the Big Bear earthquake; this is an interesting interval because it might be regarded as the "triggering time" for this large aftershock, and high strain rates were observed. Inspection shows that the interseismic strains were about 14 nε on BTSM number 1, 19 nε on BTSM number 3, 9 nrad on the NS component of tiltmeter BOA, and 65 nrad on the EW component. If we compare these values with the coseismic strains, we find that the strains are 2 to 4% of those for Landers, and 8 to 12% of those for Big Bear, while the observed bounds on tilt are much larger: 6 to 18% for Landers, and 100% compared with Big Bear.

Figure 6 shows the PFO data from the tiltmeters with

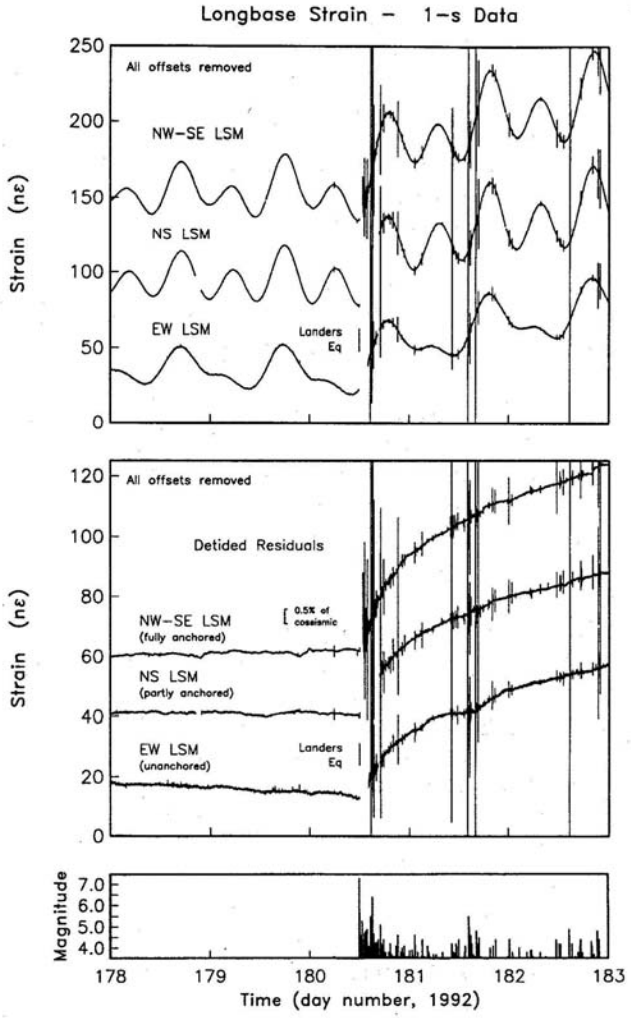

Figure 4. Six days of data from the laser strainmeters, centered at the time of the Landers mainshock. The upper panel shows the raw data, recorded at 1 Hz, but with all offsets removed; the spikes in the data are the dynamic strains from the numerous aftershocks (shown in the bottom panel, which includes all earthquakes in the area of Fig. 2). The middle panel shows the same data at an expanded scale after also removing the tides and some thermal fluctuations, both predicted from earlier data.

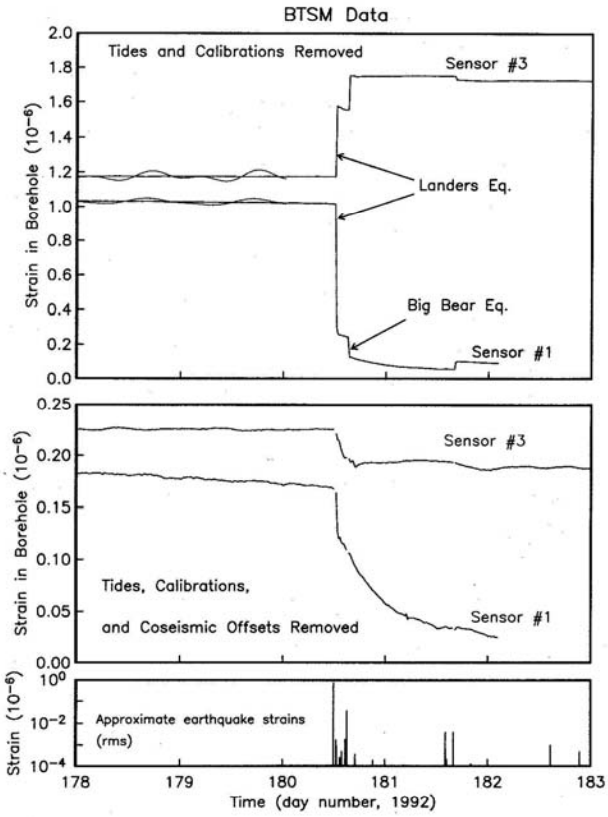

Figure 5. Data from two of the sensors of the BTSM, for the same time period as in Figure 4. In the top panel, the raw data are shown for the first 2 days, to provide a natural scale; for the entire period, the data are shown with tides (predicted using 1991 data) and calibration-induced changes removed, but with offsets retained. In the middle panel all earthquake-associated offsets have been removed to allow an increase in scale. The data shown come from individual gauges of the instrument; including the effect of borehole coupling, and in terms of the LSM extensions shown in Figure 4, the strain on gauge 1 is $0.99e_{NS} + 2.82e_{EW} - 2.11e_{NW}$, and the strain on gauge 3 is $-0.93e_{NS} - 0.02e_{EW} + 2.64e_{NW}$. The bottom panel shows the earthquake sequence, in this case in the form of the expected rms coseismic strain expected at PFO (Wyatt, 1988).

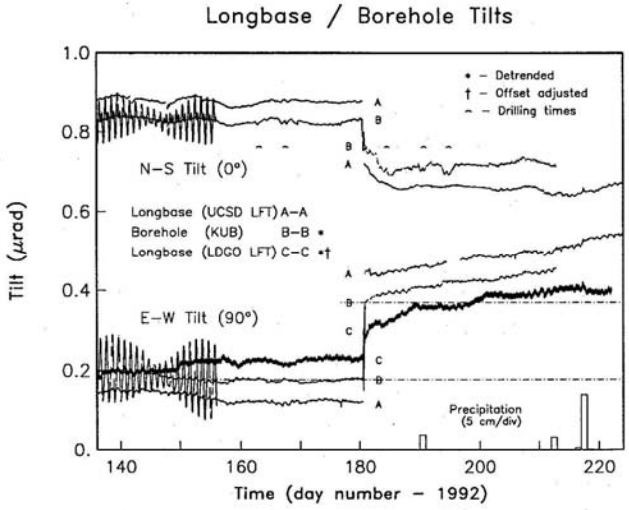

Figure 6. Tilt data for about 40 days before and after the Landers mainshock, from two components of NS tilt (one long-base and one borehole) and three components of EW tilt (two long-base instruments and the borehole sensor). As in Figure 5, the earliest data are shown with tides included. Co-seismic offsets have not been removed. The borehole sensor shows the effects of drilling about 100 m away (see Fig. 9).

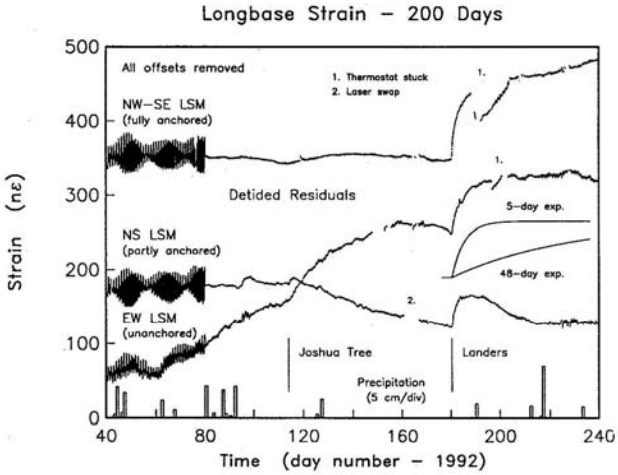

Figure 7. Laser strainmeter data for about 5 months before and 2 months after the Landers mainshock, with all co-seismic offsets removed. All corrections have been applied. Note that the NW–SE strainmeter has an optical anchor at both ends, and so gives the most stable long-term results, whereas the NS instrument is only anchored at one end, and the EW at neither; these instruments are thus more affected by end-monument instability (Wyatt, 1982). The large strain fluctuation between days 188 and 204 on the NW instrument was caused by a thermostat malfunction in one of the end vaults.

the most stable long-term records: the long-fluid tiltmeters and the Askania borehole tiltmeter. Although the latter is disturbed somewhat by nearby drilling (the drilling campaign is discussed later) its NS component shows a striking agreement with the data from the UCSD long-fluid tiltmeter: both register an initially rapid tilt rate that decays over the next few days in a manner very similar to the LSM data of Figure 4. Given the separation between these two tilt sensors (Fig. 1), and their completely different design, the similarity of their records is a strong argument for the mechanism of the postseismic deformation being at least as broadscale as PFO itself. The EW tilt measurements suggest this exponential too, and at a level closer to the LSM amounts; we suspect the EW UCSD LFT to be affected by thermal noise for a few days after the earthquake. What is particularly clear on all of the EW tilt records is a change in long-term tilt rate, relative to that seen before the Landers event: again, this similarity argues strongly for the broadscale nature of the deformation.

Figure 7 shows the long-base strains, and Figure 8 the long-base tilts, over a longer time period. Next to the postseismic response to the Landers event, the most striking aspect of Figure 7 is the possible change in strain at the time of the Joshua Tree event, which began the Landers sequence. Figure 7 also shows, for comparison, two exponential curves with different time constants (5 day and 48 day); it is clear that the postseismic strains observed immediately after the earthquakes, if treated as decaying exponentials, have a time constant closer to a few days than a few weeks. The total amount of rapid postseismic strain is, for the NW-SE LSM, ~12% of the co-seismic strain change. Figure 8 serves largely to cor-

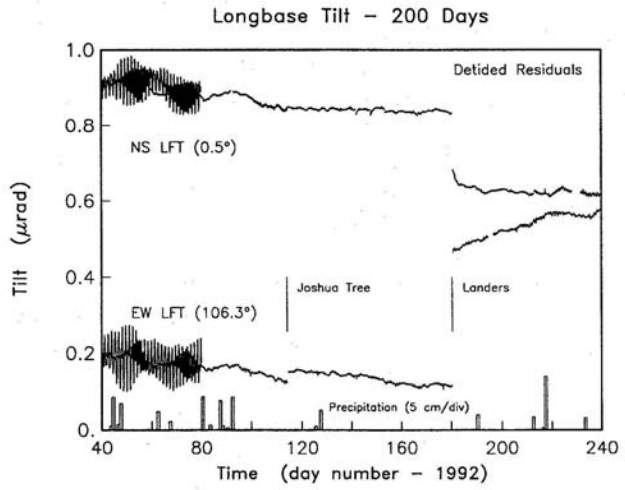

Figure 8. Long-base tiltmeter data for the same time period as the strain data in Figure 7. The LDGO long-base tilt data shown in Figure 6 have an unexplained instability during this time and so have not been shown.

roborate the features seen in the strain data (again with some allowance for noise in the EW LFT); the one additional feature is a definite change in rate in the EW LFT.

We have tried fitting the observed transients in the strain data, from a few hours to a month after the mainshock, with several functions: a decaying exponential; the power-law function of Crough and Burford (1977), which Wesson (1988) has shown corresponds to a quasi-plastic rheology; and a logarithmic function, which Marone *et al.* (1991) found to be a good approximation for afterslip propagating to the surface through a stable frictional-sliding material. Even though the strain transients look similar, the fits show substantial differences. The NW–SE data is fit much better by a log than an exponential; for the EW it is the other way around. The time constants for the exponential fits are 5 to 6 days; for the log fits less than an hour. The power-law fits both well, not surprisingly since it has more free parameters, but these are different for these two strains. Since all of these functions increase monotonically, none fits the NS strain data for more than a few days.

Interpretation and Modeling of Postseismic Observations

Because so many types of instruments show rapid strains and tilts following the Landers mainshock, these transient deformations must have occurred in the ground outside the instruments; they cannot be an artifact of any particular instrument design. It is important to realize that even very similar instruments are in fact quite independent; the three LSM's, for example, share nothing in common. Monitoring of ancillary variables that might affect some instruments shows no signal like the ones in Figure 4. The one outstanding disagreement is between the LSM data in Figure 4 and the BTSM data in Figure 5: given extension on all three LSM's, we would expect similar extensions from the three sensors of the BTSM, whereas one shows contraction and the other little postseismic signal at all. We do not think that this disagreement reflects instrumental problems, but rather a possible difference between long-base and short-base strains which we discuss later.

Given that the deformation is in the ground, what might the cause of it be? One cause would be continued deformation of the fault zone, the effect of which can be found using an elastic model for the rest of the earth, just as was done for the co-seismic offset. Another possibility is that instead it shows inelastic behavior of some part of the crust outside the fault zone. As we will see in discussing the long-term strain records, most of the time the crust is subjected only to the stresses associated with the earth tides, corresponding to strains of 3×10^{-8} or less, plus a secular strain rate of at most 3×10^{-7} yr^{-1}, and occasionally to transient strains of up to 10^{-6} from the surface waves of large teleseisms. A large earthquake, such as the Landers shock, provides transient strains of up to 10^{-4} for a few minutes, and a permanent strain change of 10^{-6} (and more closer to the fault), corresponding to permanent stress changes of 1 bar or more. The size and abruptness of this stress change is thus quite unusual, and might produce rheological effects not otherwise seen. How widespread these might be will affect our estimate of their importance: if the whole of the uppermost crust responds in a time-dependent manner to such sudden strains, it will be very difficult to make unequivocal measurements of postseismic fault slip at depth, since these can only be detected through measuring the displacements at the surface. In discussing possible mechanisms for producing these deformations through crustal anelasticity, we therefore try to distinguish between those that might be local in origin, and those that might be more widespread.

Hydraulic Fracture Opening

As is not uncommon around large earthquakes (Muir-Wood and King, 1993) the water table at PFO showed a change at the time of the Landers shock. We have continuous data from four boreholes at PFO, and manual readings from many others. Figure 9 shows data from the continuously recorded holes; a rapid transient response is visible in three of these records, as levels dropped by 0.15 to 0.3 m and then recovered. In the fourth well (UQA) the water level dropped over 5 m at the time of the Landers event. Considering the longer term, there was a general decrease in water level at the site, as the predominance of negatives values in Table 3

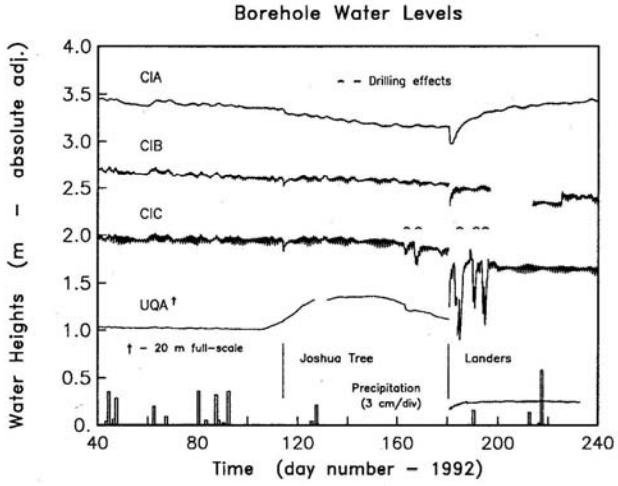

Figure 9. Water-height changes in four wells at PFO, uncorrected for tides or response to barometric pressure, for the same time period as the data in Figure 7 and Figure 8. For the locations of these wells, see Figure 2; the absolute water levels are given in Table 1. The large fluctuations in well CIC are caused by drilling 100 m away.

indicates. The data from CIC were disturbed between days 160 and 198 by a drilling operation about 100 m away, at location SDB on the site map. (This project had been postponed from April to late June to avoid interfering with possible postseismic signals from the Joshua Tree earthquake; when the Landers shock occurred it was irrevocably under-way.) Fortunately the drilling had begun before the event, so that we can say that there was no apparent effect of the drilling on the strain data before the earthquake, though it did cause repeated small fluctuations in the tiltmeter KUB, 100 m away.

A preliminary model of these water-table changes treats the bedrock at PFO as being slightly fractured (Fletcher *et al.*, 1990); on a local scale the hydrology is thus less that of a porous medium than of a sparse set of interconnecting joints. The strain changes from the earthquake will change the volumes of these joints, and the flow between them, in different ways; accelerations of the weathered near-surface rocks will cause some joints to close and others to open. We thus expect the water pressure to change irregularly throughout the fracture network. As pressures re-equilibrate and new flow rates become established the water-table heights will vary in different ways for different wells, as observed.

Evans and Wyatt (1984) related water-pressure changes to observed strain changes at PFO; the two were connected through the inflation of a large horizontal joint at 100-m depth, near the NW corner of the observatory. Since this location is common to the three long-base strainmeters, deformation there could cause the kind of postseismic transient we see in that data, while not necessarily producing large strains at the BTSM site. The LSM's might thus be recording, indirectly, only local water-table effects acting on a particular joint—explaining, in particular, why the EW LSM shows an extensional strain signal when co-seismic-matching compression is expected. However, this explanation does not mesh with the evidence of broadscale deformation discussed earlier. Also, any such local deformations would give rise to sizeable tilts (which were observed by Evans and Wyatt), something not evident in the records of a number of tiltmeters located near the NW corner. It remains possible that localized displacements at the distant ends of the LSM's are the cause, but it would then be a remarkable coincidence that these displacements all had similar time dependence. Though we cannot rule this out, it seems quite unlikely. Earlier observations of postseismic strain at PFO have always shown either no effect or else a pattern that matched the co-seismic signals (Wyatt 1988), and this has held true even for events which have caused much stronger ground shaking (e.g., Berger and Brune, 1981). Never before have we seen such high aseismic strain rates.

Table 3
Water-Level Changes 1992: 156–184

Borehole	Change (m)	Borehole	Change (m)
CIA	+0.06	GSA	−0.34
CIB	−0.11	GSB†	+0.34
CIC	−0.90	GSC†	−0.46
UQA*	−5.44	GSD†	−0.48
UQX*	−1.54‡	SDA	−0.18‡
UQY	−0.05		

*Adjacent.
†Also adjacent to one another.
‡Not measured until 1992; 218.

However, we may invoke local water-pressure changes to explain the difference between the LSM records (Fig. 4) and the BTSM data (Fig. 5). A short-base borehole system, such as the BTSM, can be affected by strain fields set up by the opening and closing of small joint surfaces nearby; such strains may be too localized to be observed farther away. If we believe that the LSM data show broadscale strains (on at least the kilometer length scale of these instruments), we must assume that strains local to the BTSM have affected its data in such a way as to produce no postseismic signal in one case, and one with opposite sign in another. We suggest that hydraulically induced joint opening in response to (probably) the large dynamic strains did occur at PFO, but that the agreement of long-base instruments, and the absence of very large local tilts, means that the localized effects discussed by Evans and Wyatt (1984) are not the primary reason for the postseismic LSM and tiltmeter signals.

Poroelastic Effects

Given that the strains we have observed have a larger scale than would be caused by localized opening of joints, they might still be caused by changes in the water table over a large scale. On a scale of kilometers, even the jointed material at Pinyon Flat can be regarded as a porous medium; one possibility is that transient strain changes are induced by changes in fluid pressure, reflecting a broadscale recovery from the change in fluid pressure induced by the co-seismic strains. We term this a poroelastic effect to distinguish it from the fracture model just discussed, in which changes in fluid flow between sparsely located joints produces local strains. The major problem with this explanation is the time constant of the postseismic signal: a change of pore pressure over several kilometers, not just between joints, would be expected to take much longer than a few days. The water-table records in Figure 9 match this; after a rapid recovery (presumably as joints near each borehole re-equilibrate), there is still a static offset, suggesting a general decrease in pore pressure that will only adjust over a very long time,—on the basis of the examples given in Muir-Wood and King (1993), many months to years.

Hydrothermal Effects

In addition to the direct elastic effects of changes in water pressure, there is also the possibility of strains in-

duced in the rock by temperature changes, as water flows from one depth to another. A general upward movement of water would bring warmer water into contact with colder rock; this will warm the rock and cause a thermoelastic strain change, in this case expansion. However, the strain signal shows general expansion, at odds with the general fall of the water table observed in the local wells (Table 3), and it also appears to be quantitatively insufficient. For a general movement of water up by a distance z, the temperature change induced in the rock will be $pC_r(dT/dz)z$, where p is the porosity (probably not more than 0.01 at Pinyon Flat), C_r is the ratio of the specific heat of water (by volume) divided by that of rock (1.8), and dT/dz is the geothermal gradient, which at PFO is 22 mK/m (Lachenbruch *et al.*, 1985). Given a coefficient of thermal expansion of $6 \times 10^{-6}\,K^{-1}$, even a 1-m rise of the water table would cause a strain of only 2×10^{-9}, much smaller than the signal we see.

Crustal Anelasticity

Even if the observed transient deformations are not caused by hydrological effects they might still reflect a crustal response apart from fault motion. The time constants for viscoelastic relaxation in the lower crust and upper mantle are generally too long to match what we have observed, but what about the upper crust? It is well known that at low pressures and room temperature rocks subjected to a constant load undergo creep that shows an initial transient of increasing rate (known as primary creep) before settling down to a steady rate of deformation (Scholz, 1990, pp. 33–34; Robertson, 1964). This primary creep has a roughly logarithmic dependence on time, corresponding well to the shape of the rapid postseismic transients observed at PFO.

A possible model for the postseismic deformations would be that an earthquake produces a sudden (co-seismic) stress change of the crust and upper mantle; the uppermost crust then undergoes stress relaxation through primary creep, with the material below it behaving elastically (at least on this short time scale). The micromechanics of this creep involve the extension of microcracks through subcritical crack growth (Atkinson and Meredith 1987; Segall 1984). This crack growth would give rise to strains within the upper crust which would produce the signals observed. Unfortunately, few tests of rock creep are set up to show relaxation from an initial stress; one case in which this does occur is in the time-dependent strain relaxation observed in overcoring stress measurements (Engelder, 1993, 1984). The strain curves observed in this case have a strong similarity, in both shape and time constant, to the postseismic deformations at PFO.

Because of the existence of a threshold for subcritical crack growth (Segall, 1984), we might not expect to see this kind of crustal response at the low strains to which the surface of the earth is typically subjected: 10^{-7} or less (except for secular strain accumulation in tectonic areas, for which it would be impossible to separate crustal response from the nature of the source). This time-dependent response would thus be present only close to, and just after, large earthquakes, as in this case we happened to be. Such effects might be even larger in areas closer to the earthquake; it remains to be seen if they could be large enough to explain the kind of near-faulting postseismic displacements seen by Shen *et al.* (1994).

Aseismic Fault Slip

From the standpoint of earthquake mechanics, the most interesting cause for the postseismic strains and tilts at PFO would be aseismic slip on faults, driven by the static strain changes from the Landers and Big Bear earthquakes; the associated stress changes have been shown (Harris and Simpson, 1992; Jaumé and Sykes, 1992; Stein *et al.*, 1992) to be up to several bars. Aseismic slip would cause the kind of large-scale deformation that we see at PFO; the challenge is to see where such deformation might be occurring in light of the PFO data and other information. Very little surface afterslip was observed for the Landers event (Sylvester, 1993), implying that any afterslip must have been deep. Frictional models of faulting (Tse and Rice, 1986; Lorenzetti and Tullis, 1989) all show some amount of deep afterslip following the actual earthquake rupture—typically on the order of 5% of the co-seismic moment in 24 hr—so this is physically reasonable.

Where might this slip have occurred? A dislocation half-space model for any particular fault segment will give the amounts of strain and tilt expected at PFO for a given amount of slip; we may then ask if the ratios between the different types of observations match (within the errors) the computed signals for PFO from dip-slip and strike-slip motion on fault segments throughout southern California. It might be thought that a shear source (such as a strike-slip fault) would not produce strains that were positive in all directions, as was observed in the PFO postseismic transients (again, we are troubled by the EW LSM results). But as Figure 10 shows, this is not so. This figure shows the candidate fault segments: those for which the ratios of NS to EW strain, and NW–SE to EW strain, are positive and lie between 0.5 and 5. Many fault segments can produce all-positive strains at PFO; though none of the faults that ruptured to create the Landers earthquake fulfill these criteria, part of the Big Bear rupture does, as well as other faults lying to the northwest of PFO. It is worth noting that the model strains from the Big Bear earthquake (Table 2) show a reasonable match to the relative amplitudes of the postseismic LSM transients. However, slip on this segment alone would not produce the observed tilts; indeed no single one of these fault segments produces the ratios between the different strains and tilts that we observed, strongly

suggesting that if fault slippage is the cause of the postseismic deformations, it must have involved several segments, not just one. That a search for single fault segments will not succeed when the source involves many segments is easily demonstrated by searching for those single segments that are compatible with the model strains and tilts in Table 2; because of the complexity of the rupture, and the proximity of PFO, none of the individual segments that did indeed rupture can mimic the results from this multi-segment model.

Long-Term Changes

In Figure 11 we show a variety of data from PFO, over the 2-yr span from 1991 through the end of 1992, primarily to illustrate the relative noise levels of different sensors and also to show limits on patterns of long-term deformation. We first show daily values of displacement computed using data from the Southern California Permanent GPS Geodetic Array (PGGA) described by Bock *et al.* (1993); the values we show here have been cleaned using a stacking algorithm developed by Dr. Shimon Wdowinski (personal comm.). These data are probably the best determination of the long-term motion of PFO, and show a clear offset at the time of the Landers and Big Bear shocks. They also, tantalizingly, suggest a postseismic displacement of 5 to 10 mm, with a somewhat longer time constant, and a much larger relative size, than what is found in the strain data. A postseismic displacement this big could not be explained by any motions local to PFO; of the mechanisms discussed in the previous section, only postseismic fault slip (and perhaps crustal anelasticity) could explain it. No other significant fluctuations are visible.

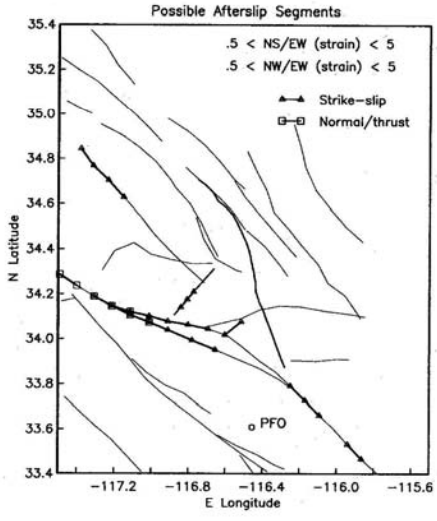

Figure 10. Faults near PFO, with segments that qualify as candidate causes of the postseismic deformation, are shown with symbols at their ends.

The bottom panel shows preliminary results of continuous GPS measurements over a shorter distance: a 14-km line from PFO west to another site (ROCH in Fig. 1). We have presented this with scales both for relative displacement and for equivalent strain; since this line runs almost exactly east–west, displacement in this direction reflects EW extension e_{11}, while NS displacement gives a measure of shear strain e_{12}. These data show co-seismic offsets that match the model results in Table 2 fairly well, being small for e_{11} and about 1 μstrain for e_{12}. We have shown these shorter-base GPS data partly for comparison with the results of continuous strain measurements; these strainmeter data show just how small the normal earth-strain fluctuations are compared with the co-seismic offsets, and with those that might be inferred from the GPS data.

Figure 12 shows four of the long-base records (leaving out the unanchored EW LSM), and one sensor of the BTSM, at an expanded scale and without co-seismic offsets. Both the LSM and BTSM data suggest, though only marginally, a change in strain rates after the Joshua Tree

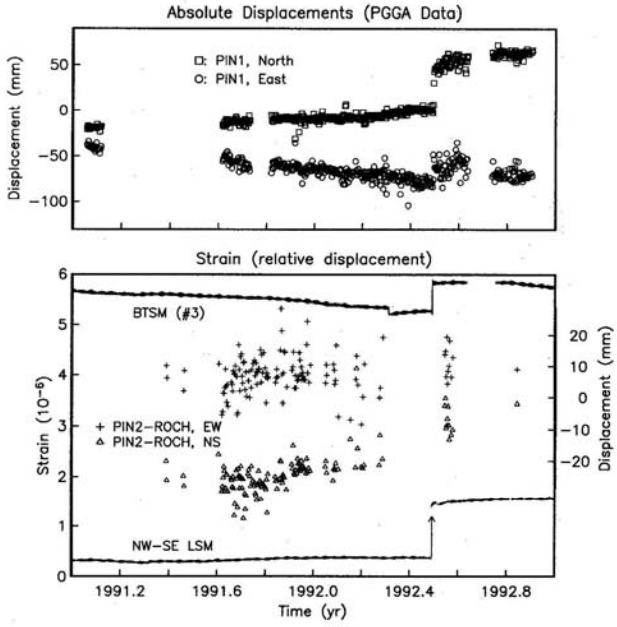

Figure 11. Various kinds of long-term deformation data from PFO. The upper panel shows the daily displacements measured by the PGGA GPS system (Bock *et al.*, 1993). The lower panel shows relative displacements determined by daily GPS solutions between PFO and another fixed station nearby (ROCH, see Fig. 1); because of the closeness of these stations we can convert these relative displacements (right axis) into strain. In addition, this panel includes the best comparable strainmeter records. On the NW–SE LSM, the co-seismic offset for the Landers earthquake is that inferred from the two-color EDM data; the offset for the Joshua Tree earthquake is not shown.

earthquake. This plot also shows that, in addition to the rapid changes seen in strain immediately following the Landers mainshock, several of the records indicate a longer-term decaying deformation. These different sorts of time behavior suggest that what we are seeing at PFO may be the result of more than one process. Some support for this comes from the GPS data described by Shen *et al.* (1994) for the area around the earthquake. Using observations which commence a few days after the mainshock (and so do not capture some of the earliest deformation) they find that a 48-day exponential provides a reasonable fit to the postseismic displacements. While such a slow decay does not agree with the initial PFO data, it does provide a good match to the later data, and the fault model developed by Shen *et al.* matches well in magnitude (though not in detail) the observations at PFO.

Conclusions

Combined, the PFO observations argue strongly for a substantial strain and tilt change following the Landers earthquake; one both far larger and more rapid than any deformations previously observed (outside of co-seismic signals). Even allowing for the likelihood that some of the observatory signals are affected by local sources of noise, we can use the array of instruments to make a strong case that this deformation extended uniformly over at least the kilometer scale of the observatory, and probably well beyond—something supported both qualitatively and quantitatively by the GPS data of Shen *et al.* (1994).

Surprisingly, the most straightforward cause for the postseismic signal, that of accelerated postseismic slip on or at the edges of the ruptured fault planes, and in proportion to the co-seismic slip, is ruled out by the observed patterns of strains and tilts at PFO, although the Big Bear rupture is suggested as a possible source. This is different from our past experience; all previous measurements at PFO have shown that the best sensors indicate either no detectable postseismic signal, or one fully in accord with the co-seismic deformation and 5 to 10% of it in size. It is important to realize that if the primary cause of the smoothly varying signals at PFO is not fault slip, these data then imply that there was very little aseismic afterslip (there being little other character to the observations), which has implications for fault physics. The definite absence of any preseismic signal is enough to rule out a large range of parameters for some models of faulting (Lorenzetti and Tullis, 1989).

Perhaps the most interesting, because novel, mechanism for the observed postseismic signals would be transient creep of the upper part of the crust in response to the large stress change imposed by the elastic rebound that drives the earthquake: stress-induced changes in microcracks in materials not under high confining pressures. Further modeling will be needed to determine how large an effect such as this might reasonably be; if it should turn out to be large in the area of significant stress change, the unequivocal observation of postseismic fault motion might remain forever impossible, being obscured by crustal response in the only locations where it is large enough to rise above instrumental noise.

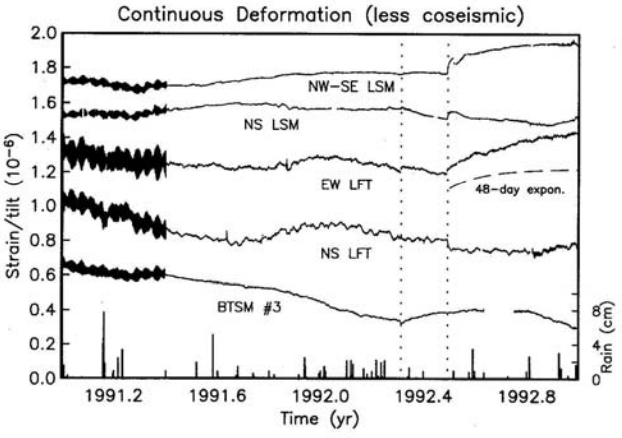

Figure 12. Data from several of the long-base sensors, and also the most reliable of the BTSM records. Co-seismic offsets have been removed. See Figure 5 for a description of the relation between the BTSM and LSM data. With the exception of a possible transient following the Joshua Tree shock (occurring at first dotted vertical line), there are no indications of any anomalous strains other than the Landers postseismic strains.

Acknowledgments

This paper is dedicated to the memory of Leo Weuve, caretaker (and much more) at PFO beginning in 1972; he saw the beginning of the Landers/Joshua Tree sequence, and was able to leave the observatory in good shape for its culmination. We thank many of the other investigators, whose efforts have combined at PFO, for the use of their data; in particular: John Beavan (Lamont-Doherty), Yehuda Bock and Shimon Wdowinski (UCSD), John Langbein (U.S. Geological Survey), Judah Levine and Mary Kohl (University of Colorado), and Walter Züm (Karlsruhe University). Joseph Jarboe and Ross Gwyther did much of the data processing needed to produce and understand the records presented here; for assistance in running the observatory we also are indebted to Steve Bralla and Hadley Johnson. Jim Happer processed the PFO/ROCH data. Kerry Sieh provided the digitized fault-rupture data used in Figure 2, and Ruth Harris and Bob Simpson that used in Figure 10. Malcolm Johnston suggested the possibility of hydrothermal effects. We thank Tim Dixon and an anonymous reviewer for providing excellent suggestions in how to improve this article. This research effort was supported by the National Science Foundation, the U.S. Geological Survey and the Southern California Earthquake Center.

References

Agnew, D. C. (1986). Strainmeters and tiltmeters, *Rev. Geophys.* **24**, 579–624.

Agnew, D. C. and F. Wyatt (1989). The 1987 Superstition Hills earthquake sequence: strains and tilts at Piñon Flat Observatory, *Bull. Seism. Soc. Am.* **79**, 480–492.

Abercrombie, R. E. and J. Mori (1994). Local observations of the onset of a large earthquake: 28 June 1992 Landers, California, *Bull. Seism. Soc. Am.* **84**, no. 3, 725–734.

Atkinson, B. K. and P. G. Meredith (1987). The theory of subcritical crack growth with applications to minerals and rocks, in *Fracture Mechanics of Rock*, B. Atkinson (Editor), Academic Press, San Diego, California, 111–166.

Berger, J. and J. Brune (1981). Studies of the seismic and crustal deformation patterns of an active fault: Piñon Flat Observatory, *Summaries of Technical Reports, NEHRP* **XI**, 327–330.

Bilham, R. G., R. Plumb, and J. Beavan (1979). Design considerations in an ultra-stable, long baseline tiltmeter—results from a laser tiltmeter, in Terrestrial and Space Techniques, *Earthquake Prediction Research*, A. Vogel (Editor), Friedr. Vieweg and Sohn, Wiesbaden, 235–254.

Bock, Y. and S. Shimada (1990). Continuously monitoring GPS networks for deformation measurements, in *Global Positioning System: An Overview*, Y. Bock (Editor), Springer-Verlag, New York, 40–56.

Bock, Y., D. C. Agnew, P. Fang, J. F. Genrich, B. H. Hager, T. A. Herring, R. W. King, S. Larsen, J. B. Minster, K. Stark, S. Wdowinski, and F. K. Wyatt (1993). Detection of coseismic deformation in southern California using continuous Global Positioning System measurements, *Nature* **361**, 337–340.

Crough, S. T. and R. O. Burford (1977). Empirical function for fault-creep events, *Tectonophysics* **42**, 53–59.

Engelder, T. (1984). The time-dependent strain relaxation of Algerie Granite, *Int. J. Rock Mech. Mining Sci.* **21**, 63–73.

Engelder, T. (1993). *Stress Regimes in the Lithosphere*, Princeton University Press, Princeton.

Evans, K. and F. Wyatt (1984). Water table effects on the measurement of earth strain, *Tectonophysics* **108**, 323–337.

Fletcher, J., T. Fumal, H.-P. Liu, and J. C. Carroll (1990). Near-surface velocities and attenuation at two boreholes near Anza, California from logging data, *Bull. Seism. Soc. Am.* **80**, 807–831.

Gladwin, M. T. (1984). High-precision multicomponent borehole deformation monitoring, *Rev. Sci. Instr.* **55**, 2011–2016.

Gladwin, M. T., R. L. Gwyther, R. G. Hart, M. Francis, and M. J. S. Johnston (1987). Borehole tensor strain measurements in California, *J. Geophys. Res.* **92**, 7981–7988.

Gladwin, M. T., R. L. Gwyther, J. W. Higbie, and R. G. Hart (1991). A medium term precursor to the Loma Prieta earthquake? *Geophys. Res. Lett.* **18**, 1377–1380.

Gladwin, M. T. and R. Hart (1985). Design parameters for borehole strain instrumentation, *Pure Appl. Geophys.* **123**, 59–80.

Gwyther, R. L., M. T. Gladwin, and R. Hart (1992). A shear-strain anomaly following the Loma Prieta earthquake, *Nature* **356**, 142–144.

Happer, J., D. Agnew, Y. Bock, H. Johnson, K. Stark, and F. Wyatt (1991). Results from continuous GPS measurements over a 14-km line, *EOS*, 1991 Fall. Meeting Suppl., 118.

Harris, R. A. and R. W. Simpson (1992). Changes in static stress on the southern California faults after the 1992 Landers earthquake, *Nature* **360**, 251–254.

Hauksson, E., L. M. Jones, K. Hutton, and D. Eberhart-Phillips (1993). The 1992 Landers earthquake sequence: seismological observations, *J. Geophys. Res.* **98**, 19835–19858.

Hudnut, K., Y. Bock, M. Cline, P. Fang, J. Freymuller, K. Gross, D. Jackson, S. Larson, M. Lisowski, Z. Shen, and J. Savage (1994). Coseismic deformations in the Landers earthquake sequence, *Bull. Seism. Soc. Am.* (in press).

Jaumé, S. and L. Sykes (1992). Changes in state of stress on the southern San Andreas fault resulting from the California earthquake sequence of April to June 1992, *Science* **258**, 1325–1328.

Johnson, H. O., D. C. Agnew, and K. Hudnut (1994). Extremal bounds on earthquake moment from geodetic data: application to the Landers earthquake, *Bull. Seism. Soc. Am.* **84**, no. 3, 660–667.

Johnston, M., A. T. Linde, M. T. Gladwin, and R. Borcherdt (1987). Fault failure with moderate earthquakes, *Tectonophysics* **144**, 189–206.

Johnston, M. J. S., A. T. Linde, and M. T. Gladwin (1990). Near-field high resolution strain measurements prior to the October 18, 1989, Loma Prieta M_L 7.1 earthquake, *Geophys. Res. Lett.* **8**, 1777–1780.

Kohl, M. L. and J. Levine (1993). Measuring low frequency tilts, *J. Res. N.I.S.T.* **98**, 191–202.

Lachenbruch, A. H., J. H. Sass, and S. P. Galanis (1985). Heat flow in southernmost California and the origin of the Salton trough, *J. Geophys. Res.* **90**, 6709–6735.

Langbein, J. O., M. F. Linker, A. F. McGarr, and L. E. Slater (1987). Precision of two-color geodimeter measurements: results from 15 months of observations, *J. Geophys. Res.* **92**, 11644–11656.

Lorenzetti, E. and T. Tullis (1989). Geodetic predictions of a strike-slip fault model: implications for intermediate- and short-term earthquake prediction, *J. Geophys. Res.* **94**, 12343–12362.

Marone, S., C. Scholz, and R. Bilham (1991). On the mechanics of earthquake afterslip, *J. Geophys. Res.* **96**, 8441–8450.

Muir-Wood, R and G. C. P. King (1993). Hydrological signatures of earthquake strain, *J. Geophys. Res.* **98**, 22035–22068.

Robertson, E. C. (1964). Viscoelasticity of rocks, in *State of Stress in the Earth's Crust*, W. Judd (Editor), Elsevier, New York, 181–224.

Scholz, C. H. (1990). *The Mechanics of Earthquakes and Faulting*, Cambridge University Press, Cambridge, United Kingdom.

Segall, P. (1984). Rate-dependent extensional deformation resulting from crack growth in rock, *J. Geophys. Res.* **89**, 4185–4195.

Shen, Z.-K., D. Jackson, Y. Feng, M. Cline, M. Kim, P. Fang, and Y. Bock (1994). Postseismic deformation following Landers Earthquake, California, June 28, 1992, *Bull. Seism. Soc. Am.* **84**, no. 3, 780–791.

Stein, R., G. King, and J. Lin (1992). Change in failure stress on the southern San Andreas fault system caused by the 1992 magnitude = 7.4 Landers earthquake, *Science* **258**, 1328–1332.

Sylvester, A. G. (1993). Investigation of nearfield postseismic slip following the M_W 7.3 Landers earthquake sequence of 28 June 1992, California, *Geophys. Res. Lett.* **20**, 1079–1082.

Tse, S. T. and J. R. Rice (1986). Crustal earthquake instability in relation to the depth variation of frictional slip properties, *J. Geophys. Res.* **91**, 9452–9472.

Wesson, R. L. (1988). Dynamics of fault creep, *J. Geophys. Res.* **93**, 8929–8951.

Wyatt, F. (1982). Displacements of surface monuments: horizontal motion, *J. Geophys. Res.* **87**, 979–989.

Wyatt, F. (1988). Measurements of coseismic deformation in southern California: 1972–1982, *J. Geophys. Res.* **93**, 7923–7942.

Wyatt, F., K. Beckstrom, and J. Berger (1982). The optical anchor—A geophysical strainmeter, *Bull. Seism. Soc. Am.* **72**, 1701–1715.

IGPP 0225
University of California, San Diego
La Jolla, California 92093-0225
(F.K.W., D.C.A.)

Department of Physics
University of Queensland
St. Lucia, Queensland 4067
Australia
(M.G.)

Manuscript received 5 August 1993.